
This copy is for your personal, non-commercial use only.

If you wish to distribute this article to others, you can order high-quality copies for your colleagues, clients, or customers by [clicking here](#).

Permission to republish or repurpose articles or portions of articles can be obtained by following the guidelines [here](#).

The following resources related to this article are available online at www.sciencemag.org (this information is current as of September 1, 2014):

Updated information and services, including high-resolution figures, can be found in the online version of this article at:

<http://www.sciencemag.org/content/344/6187/1001.full.html>

Supporting Online Material can be found at:

<http://www.sciencemag.org/content/suppl/2014/05/28/344.6187.1001.DC1.html>

This article **cites 48 articles**, 6 of which can be accessed free:

<http://www.sciencemag.org/content/344/6187/1001.full.html#ref-list-1>

This article appears in the following **subject collections**:

Physics, Applied

http://www.sciencemag.org/cgi/collection/app_physics

This study experimentally evaluates the long-term impact of an early childhood psychosocial stimulation intervention on earnings in a low-income country. Twenty years after the intervention was conducted, we find that the earnings of the stimulation group are 25% higher than those of the control group and caught up to the earnings of a nonstunted comparison group. These findings show that a simple psychosocial stimulation intervention in early childhood for disadvantaged children can have a substantial effect on labor market outcomes and can compensate for developmental delays. The estimated impacts are substantially larger than the impacts reported for the U.S.-based interventions, suggesting that ECD interventions may be an especially effective strategy for improving long-term outcomes of disadvantaged children in developing countries.

REFERENCES AND NOTES

- P. R. Huttenlocher, *Brain Res.* **163**, 195–205 (1979).
- P. R. Huttenlocher, *Neural Plasticity: The Effects of Environment on the Development of the Cerebral Cortex* (Harvard Univ. Press, Cambridge, MA, 2002).
- R. A. Thompson, C. A. Nelson, *Am. Psychol.* **56**, 5–15 (2001).
- E. I. Knudsen, J. J. Heckman, J. L. Cameron, J. P. Shonkoff, *Proc. Natl. Acad. Sci. U.S.A.* **103**, 10155–10162 (2006).
- J. J. Heckman, *Science* **312**, 1900–1902 (2006).
- J. J. Heckman, *Econ. Inq.* **46**, 289–324 (2008).
- P. Carneiro, J. J. Heckman, in *Inequality in America: What Role for Human Capital Policies?* J. J. Heckman, A. B. Krueger, B. M. Friedman, Eds. (MIT Press, Cambridge, MA, 2003), pp. 77–239.
- F. Cunha, J. J. Heckman, L. J. Lochner, D. V. Masterov, in *Handbook of the Economics of Education*, E. A. Hanushek, F. Welch, Eds. (North-Holland, Amsterdam, 2006), chap. 12, pp. 697–812.
- G. J. van den Berg, M. Lindeboom, F. Portrait, *Am. Econ. Rev.* **96**, 290–302 (2006).
- D. Almond, L. Edlund, H. Li, J. Zhang, Long-term effects of the 1959–1961 China famine: Mainland China and Hong Kong, *Working Paper 13384*, National Bureau of Economic Research (2007).
- H. Bleakley, *Q. J. Econ.* **122**, 73–117 (2007).
- S. L. Maccini, D. Yang, *Am. Econ. Rev.* **99**, 1006–1026 (2009).
- D. Almond, J. Currie, in *Handbook of Labor Economics*, O. Ashenfelter, D. Card, Eds. (Elsevier, North Holland, 2011), vol. 4B, chap. 15, pp. 1315–1486.
- P. L. Engle et al., *Lancet* **369**, 229–242 (2007).
- P. L. Engle et al., *Lancet* **378**, 1339–1353 (2011).
- J. J. Heckman, *Res. Econ.* **54**, 3–56 (2000).
- S. Grantham-McGregor et al., *Lancet* **369**, 60–70 (2007).
- S. P. Walker et al., *Lancet* **369**, 145–157 (2007).
- C. Paxson, N. Schady, *J. Hum. Resour.* **42**, 49 (2007).
- L. C. Fernald, P. Kariger, M. Hidrobo, P. J. Gertler, *Proc. Natl. Acad. Sci. U.S.A.* **109** (suppl. 2), 17273–17280 (2012).
- J. Heckman, S. H. Moon, R. Pinto, P. Savellyev, A. Yavitz, *Quant. Econom.* **1**, 1–46 (2010).
- J. J. Heckman, S. H. Moon, R. Pinto, P. A. Savellyev, A. Yavitz, *J. Public Econ.* **94**, 114–128 (2010).
- A. J. Reynolds, S.-R. Ou, J. W. Topitzes, *Child Dev.* **75**, 1299–1328 (2004).
- A. J. Reynolds et al., *Arch. Pediatr. Adolesc. Med.* **161**, 730–739 (2007).
- A. J. Reynolds, J. A. Temple, S.-R. Ou, I. A. Arteaga, B. A. B. White, *Science* **333**, 360–364 (2011).
- F. A. Campbell, C. T. Ramey, E. Pungello, J. Sparling, S. Miller-Johnson, *Appl. Dev. Sci.* **6**, 42–57 (2002).
- F. A. Campbell et al., *Dev. Psychol.* **48**, 1033–1043 (2012).
- F. Campbell et al., *Science* **343**, 1478–1485 (2014).
- A. Aughinbaugh, *J. Hum. Resour.* **36**, 641 (2001).
- E. Garces, D. Thomas, J. Currie, *Am. Econ. Rev.* **92**, 999–1012 (2002).
- G. Psacharopoulos, H. A. Patrinos, *Educ. Econ.* **12**, 111–134 (2004).
- S. M. Grantham-McGregor, C. A. Powell, S. P. Walker, J. H. Himes, *Lancet* **338**, 1–5 (1991).
- There are, however, experimental studies that show that early-life nutritional interventions also have substantial impacts on earnings (44).
- S. P. Walker, S. M. Chang, M. Vera-Hernández, S. Grantham-McGregor, *Pediatrics* **127**, 849–857 (2011).
- S. P. Walker, C. A. Powell, S. M. Grantham-McGregor, *Eur. J. Clin. Nutr.* **44**, 527–534 (1990).
- S. P. Walker, S. M. Chang, C. A. Powell, S. M. Grantham-McGregor, *Lancet* **366**, 1804–1807 (2005).
- S. P. Walker, S. M. Chang, M. Vera-Hernández, S. Grantham-McGregor, *Pediatrics* **127**, 849–857 (2011).
- S. P. Walker, S. M. Grantham-McGregor, C. A. Powell, S. M. Chang, *J. Pediatr.* **137**, 36–41 (2000).
- J. M. Robins, A. Rotnitzky, L. P. Zhao, *J. Am. Stat. Assoc.* **89**, 846–866 (1994).
- J. P. Romano, M. Wolf, *J. Am. Stat. Assoc.* **100**, 94–108 (2005).
- B. M. Caldwell, *Pediatrics* **40**, 46–54 (1967).
- B. M. Caldwell, R. H. Bradley, *HOME Observation for Measurement of the Environment* (University of Arkansas at Little Rock, Little Rock, AR, 1984).
- S. M. Grantham-McGregor, S. P. Walker, S. M. Chang, C. A. Powell, *Am. J. Clin. Nutr.* **66**, 247–253 (1997).
- J. Hoddinott, J. A. Maluccio, J. R. Behrman, R. Flores, R. Martorell, *Lancet* **371**, 411–416 (2008).

ACKNOWLEDGMENTS

We gratefully acknowledge research support from the World Bank Strategic Impact Evaluation Fund; the American Bar Foundation; The Pritzker Children's Initiative; grants R37HD065072 and

ROIHD54702 from the Eunice Kennedy Shriver National Institute of Child Health and Human Development; the Human Capital and Economic Opportunity Global Working Group—an initiative of the Becker Friedman Institute for Research in Economics funded by the Institute for New Economic Thinking (INET); a European Research Council grant hosted by University College Dublin; DEVHEALTH 269874; and an anonymous funder. We have benefited from comments of participants in seminars at the University of Chicago; University of California, Berkeley; Massachusetts Institute of Technology; the 2011 LACEA Meetings in Santiago, Chile; and the 2013 AEA Meetings. We thank the study participants for their continued cooperation and willingness to participate, and S. Pellington for conducting the interviews. The authors have not received any compensation for the research nor do they have any financial stake in the analyses reported here. Replication data for this article have been deposited at Interuniversity Consortium for Political and Social Research (ICPSR) and can be accessed at <http://doi.org/10.3886/E2402V1>.

SUPPLEMENTARY MATERIALS

www.sciencemag.org/content/344/6187/998/suppl/DC1
Materials and Methods
Figs. S1 and S2
Tables S1 to S17
References (45–50)

22 January 2014; accepted 6 May 2014
10.1126/science.1251178

SOLAR CELLS

Coherent ultrafast charge transfer in an organic photovoltaic blend

Sarah Maria Falke,^{1,2*} Carlo Andrea Rozzi,^{3*} Daniele Brida,^{4,5} Margherita Maiuri,⁴ Michele Amato,⁶ Ephraim Sommer,^{1,2} Antonietta De Sio,^{1,2} Angel Rubio,^{7,8} Giulio Cerullo,⁴ Elisa Molinari,^{3,9†} Christoph Lienau^{1,2‡}

Blends of conjugated polymers and fullerene derivatives are prototype systems for organic photovoltaic devices. The primary charge-generation mechanism involves a light-induced ultrafast electron transfer from the light-absorbing and electron-donating polymer to the fullerene electron acceptor. Here, we elucidate the initial quantum dynamics of this process. Experimentally, we observed coherent vibrational motion of the fullerene moiety after impulsive optical excitation of the polymer donor. Comparison with first-principle theoretical simulations evidences coherent electron transfer between donor and acceptor and oscillations of the transferred charge with a 25-femtosecond period matching that of the observed vibrational modes. Our results show that coherent vibronic coupling between electronic and nuclear degrees of freedom is of key importance in triggering charge delocalization and transfer in a noncovalently bound reference system.

The currently accepted model for the basic working principle of a bulk-heterojunction organic solar cell (1, 2), comprising a conjugated polymer donor and an electron acceptor material, relies on four elementary steps: (i) photon absorption, creating a spatially localized, Coulomb-bound electron-hole pair (exciton) in the donor phase; (ii) exciton diffusion to the donor/acceptor interface; (iii) exciton dissociation at the interface leading to the formation of a charge-separated state (3, 4), often called charge-transfer exciton or polaron pair; and (iv) dissociation of the polaron pair into free charges and their transport to the electrodes.

In this work, we focused on the dynamics of the primary light-induced steps, (i) and (iii),

which lead to a charge-separated state in organic photovoltaic (OPV) materials and represent the key process in OPV cells. Over the past years, charge photogeneration has been investigated in several technologically relevant materials, such as blends of polyphenylene-vinylene (5, 6), polythiophene (7, 8), or low band gap polymers (9, 10) with fullerene derivatives. In all of these systems, it is now accepted that charge separation is an ultrafast process occurring on a sub-100-fs time scale. So far the experimental studies on charge photogeneration in OPV materials have mainly been described within the framework of an incoherent transfer model (11, 12), giving a rate constant for the transfer process. These rate constants may be enhanced by hot exciton dissociation

(10, 13). Recently, several theoretical studies have simulated the electronic structure (14–16) and charge transfer in this class of systems (17–19) by ab initio and/or model approaches and point toward an important role of vibronic quantum coherence for the charge separation (17, 18). In biological (20–22) and in some prototypical artificial (23, 24) light-harvesting systems, quantum coherence phenomena have recently been observed experimentally, and this has marked a breakthrough in the description of the primary processes of energy and charge transfer in macromolecular complexes. However, still very little is known about the role of quantum coherence at room temperature in the earliest stage of the dynamics in technologically relevant OPV materials. Recent experiments found evidence for an ultrafast long-range charge separation in such systems but could not differentiate between coherent and incoherent charge-transfer models (25).

We studied the ultrafast optical response of a reference OPV material system by combining high time-resolution pump-probe spectroscopy and time-dependent density functional theory (TDDFT) simulations. We observed that the ultrafast electron transfer from the polymer triggers coherent vibrational motion of the fullerene and constitutes the primary step of the photoinduced charge-separation process.

We investigated thin films of the conjugated polymer poly-3-hexylthiophene (P3HT), the fullerene derivative [6,6]-phenyl-C₆₁ butyric acid methyl ester (PCBM), and P3HT:PCBM blends with 1:1 mixing ratio in weight, prepared by spin coating from chlorobenzene solutions. Such blended films are a prototypical material for OPV cells (26, 27), and power conversion efficiencies of up to 5% have been reported (28). The absorption spectrum of a P3HT:PCBM blend (Fig. 1A, solid line) appears mainly as a linear superposition of those of the two separate components (Fig. 1B, solid lines) (29), indicating that no direct charge-transfer transitions occur in the ground state. Weak absorption features below the lowest excitonic resonance (30, 31) may reflect defects or

charge-transfer exciton transitions associated to specific local configurations.

In order to gain insight into the primary photo-induced charge-transfer dynamics of the blend, we performed ultrafast spectroscopic studies on such thin films by using a two-color pump-probe spectrometer providing independently tunable pulses (32). Because the charge-carrier photogeneration in P3HT:PCBM blends is essentially independent of temperature (33), all experiments were performed at room temperature. The overall time resolution of the setup is better than 15 fs. Pump pulses centered at 540 nm resonantly excite the π - π^* absorption band of P3HT (30, 34), whereas broadband probe pulses monitor the transient absorption in the blue-to-green wavelength range.

Figure 2A shows a measurement of the pump-induced change in optical transmission ($\Delta T/T$) for the P3HT:PCBM blend as a function of probe wavelength λ and pump-probe delay τ . A similar measurement for the pristine P3HT film is reported in the supplementary materials. For probe wavelengths between 500 and 525 nm, the signal is in both samples dominated by ground-state bleaching of the optically excited exciton transition in the polymer. In the shorter wavelength range, the dynamics are substantially different. There, the exciton bleaching of the polymer becomes less prominent, and we have, in the blend, access to an additional stimulated emission signal

from the fullerene or intermediate states. In this region, the blended sample displayed an additional and fast-decaying component on a 100-fs time scale (supplementary materials), which can be assigned to an ultrafast charge transfer from the polymer to the fullerene. This time scale is in agreement with previous reports on similar blends (5) and with the results of detailed pump-probe measurements covering the probe wavelength range between 550 and 1400 nm. These results (supplementary materials) show that a substantial fraction of all photogenerated excitons in the blend undergo rapid charge separation on a 50- to 70-fs time scale.

For both the pristine P3HT and the blend samples, the $\Delta T/T$ map (Fig. 2A and fig. S2) shows a pronounced oscillatory contrast throughout the entire visible range. We further analyzed these $\Delta T/T$ data by taking the Fourier transform of the oscillatory component after subtraction of a slowly varying background. In the 500- to 520-nm wavelength region (Fig. 2, B and C), we observed, for both the polymer and the blend, the characteristic C=C stretching frequency of the polymer (1450 cm^{-1} , corresponding to a vibrational period of 23 fs). For shorter probe wavelengths, the behavior became more complex: In the pristine film we saw almost no contrast, whereas in the blended film we detected a strong oscillatory component at a higher frequency of 1470 cm^{-1} . This frequency corresponds to the pinch mode dominating the Raman spectrum

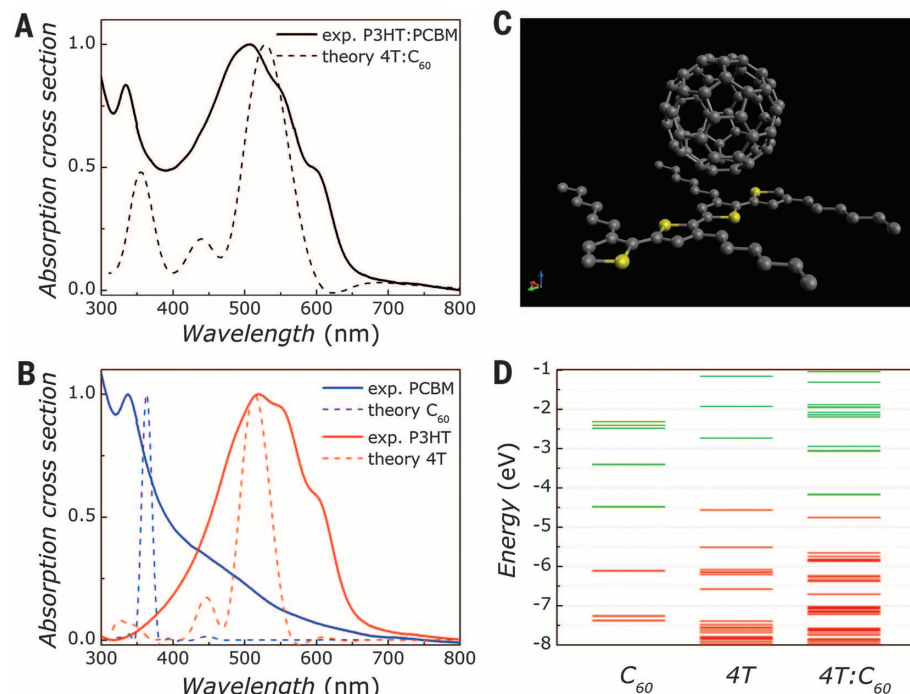


Fig. 1. Linear optical and electronic properties of the materials. (A) Normalized thin-film absorption cross section of P3HT:PCBM 1:1 ratio in weight (solid) together with the theoretical 4T:C₆₀ absorption spectrum (dashed). No signature of ground-state mixing in the blend is observed. (B) Normalized experimental absorption cross sections of PCBM (solid blue) and pristine P3HT (solid red) and the theoretical absorption of C₆₀ (dashed blue) and 4T (dashed red). (C) Molecular structure of the P3HT:C₆₀ blend system. The sulfur atoms belonging to the thiophene rings are depicted in yellow, whereas the carbon atoms are shown in gray. (D) Calculated electronic Kohn-Sham levels of (from left to right) C₆₀, 4T, and 4T:C₆₀ blend.

¹Institut für Physik, Carl von Ossietzky Universität, 26129 Oldenburg, Germany. ²Center of Interface Science, Carl von Ossietzky Universität, 26129 Oldenburg, Germany. ³Istituto Nanoscienze–Consiglio Nazionale delle Ricerche (CNR), Centro S3, via Campi 213a, 41125 Modena, Italy. ⁴Istituto di Fotonica e Nanotecnologie–CNR, Dipartimento di Fisica, Politecnico di Milano, 20133 Milano, Italy. ⁵Department of Physics and Center for Applied Photonics, University of Konstanz, 78457 Konstanz, Germany. ⁶Institut d'Électronique Fondamentale, UMR8622, CNRS, Université Paris-Sud, 91405 Orsay, France. ⁷Nano-Bio Spectroscopy Group and European Theoretical Spectroscopy Facility Scientific Development Centre, Departamento Física de Materiales, Universidad del País Vasco (UPV), Centro de Física de Materiales Consejo Superior de Investigaciones Científicas–UPV/Euskal Herriko Unibertsitatea–Materials Physics Center and Donostia International Physics Center, Avenida Tolosa 72, 20018 San Sebastián, Spain. ⁸Fritz-Haber-Institut der Max-Planck-Gesellschaft, 14195 Berlin, Germany. ⁹Dipartimento di Scienze Fisiche, Informatiche e Matematiche, Università di Modena e Reggio Emilia, via Campi 213a, 41125 Modena, Italy.

*These authors contributed equally to this work. †Corresponding author. E-mail: elisa.molinari@unimore.it (E.M.); christoph.lienau@uni-oldenburg.de (C.L.)

of the PCBM film (35, 36). Also in the 470- to 480-nm probe wavelength range, we found vibrational characteristics of the fullerene. There, we saw a weak vibrational mode at 1289 cm^{-1} , corresponding to the $T_{1g}(3)$ mode of PCBM. Control experiments on pristine PCBM films (fig. S3) did not show any evidence of coherence, thus ruling out direct PCBM excitation as a cause for the observed oscillations at 1470 cm^{-1} . These results are difficult to reconcile with an incoherent charge-transfer model, which predicts a gradual and monotonous buildup of charge on the fullerene acceptor on a 100-fs time scale that will not trigger coherent motion on a faster time scale. Also, they cannot be interpreted in terms of an incoherent charge transfer taking place within less than one vibrational period (23 fs) because such a fast transfer is neither seen in the $\Delta T/T$ data in the supplementary materials nor consistent with finding essentially the same linewidths in the absorption spectra of the pristine P3HT film and the blend. Instead, they provide evidence for a coherent charge transfer mediated by strong vibronic couplings between polymer and fullerene.

To analyze the experimental observations, we have performed first-principle calculations (25) on the simplest possible model of the experimentally studied thin-film blend, a periodic crystal of charge transfer dimers. P3HT has been substituted with a C_{60} molecule, and the alkyl side chains on the polymer have been removed in order to reduce the numerical complexity, checking that this does not affect the ground-state properties of the system. By using density functional theory (DFT) at the local density approximation (LDA) level, we relaxed the ground state of the system and found an equilibrium

distance of 3.2 \AA between 4T and C_{60} . The Kohn-Sham electron energy levels of the 4T: C_{60} unit are shown in Fig. 1D together with the electronic structure of the isolated C_{60} and 4T, all aligned to vacuum. The orbital localization shows a highest occupied molecular orbital (HOMO) with 96% localization on the thiophene chain and a lowest unoccupied molecular orbital (LUMO) almost fully localized on the fullerene. The lowest-lying available single-particle thiophene excitation corresponds to a HOMO-to-LUMO transition with 94% localization on the polymer. Steady-state optical absorption spectra (37, 38) of the blend and the isolated components are depicted in Fig. 1, A and B, respectively. The absorption cross sections of both the isolated moieties and of 4T: C_{60} are in good agreement with the experimentally observed ones. They consist of two distinct absorption bands, centered at 528 and 354 nm, that correspond to thiophene and fullerene excitations, respectively. This calculation supports the picture of a system composed of moieties that are weakly interacting in their ground states.

TDDFT simulations of the dynamics of the photoexcited 4T: C_{60} model system were performed by imposing periodic boundary conditions in order to mimic the experimental configuration of a blended thin film. We interrogated the system dynamics by assuming an initial instantaneously excited electronic state corresponding to the removal of an electron from the polymer HOMO and the creation of an electron in the polymer LUMO. We chose as initial condition a Maxwellian distribution of random nuclear velocities to approximate the experimental room-temperature environment. We observed that an electron is transferred to C_{60} with 60% probability

within 97 fs, in good agreement with experimental findings (7, 8). Moreover, the charge-transfer probability, taken as the spatially integrated excess charge density on the C_{60} , oscillated in time with a period of about 25 ± 4 fs (Fig. 3A). This period approximately matches the oscillation frequency observed in the experiments. A useful insight into the charge delocalization mechanism is gained by looking at the first few time-dependent Kohn-Sham eigenvalues above the 4T HOMO (Fig. 3C). The continuous purple line represents the 4T LUMO, occupied at time 0 by one electron removed from the 4T HOMO (purple broken line). Its energy undergoes pronounced oscillations in antiphase with the C_{60} LUMO. At each crossing of the two levels, the charge density is free to move through the system (Fig. 3C), causing a transient peak in the current flowing between 4T and C_{60} and back (Fig. 3A). Instead, the current flow is suppressed when 4T and C_{60} LUMOs are energetically detuned, resulting in a periodic variation of the current flow and thus an oscillatory modulation of amount of charge transferred to the C_{60} moiety. In the long term, the charge will be localized on the acceptor both by a nuclear rearrangement and by energy dissipation. This regime, however, is out of the scope of the present calculations. Our simulations thus predict that vibronic coupling is necessary for charge transfer to occur and indicate that this coupling is responsible for dynamically driving 4T and C_{60} LUMOs in resonance, explaining the coherent oscillations of the transferred charge. In fact, the electronic excitation remains fully localized on the polymer when keeping the ions in fixed positions (fig. S4).

The charge separation is further analyzed by examining the time-dependent dipole moment of the system (Fig. 3B). Its z component is oriented along the axis from the polymer to the C_{60} and oscillates in phase with the displaced charge, whereas the y component shows weakly anticorrelated oscillations along the polymer chain. This again points to vibronic coherence and a periodic charge flow between polymer and fullerene. The dynamics of the charge separation process are nicely visualized by displaying the time evolution of the electronic density projected onto the coupled LUMO orbitals of the blend (Fig. 3, D to F, and movie S1). This charge density is created by photoexcitation at time zero and is initially fully localized on the polymer (Fig. 3D). As the time evolves, the charge density delocalizes between polymer and C_{60} , and the degree of fractional charge on both moieties displays anticorrelated temporal oscillations. At the end of the simulation, it is shared between donor and acceptor (Fig. 3F).

In the simulations, we also analyzed the time-dependent ionic displacements (movie S2) and found that the photoexcitation of 4T promotes vibrational motion of the C_{60} with similar oscillation period as is found in the charge transfer probability. This is consistent with the experimental observation of collective vibronic coherence of the fullerene triggered by impulsive photoexcitation of the polymer.

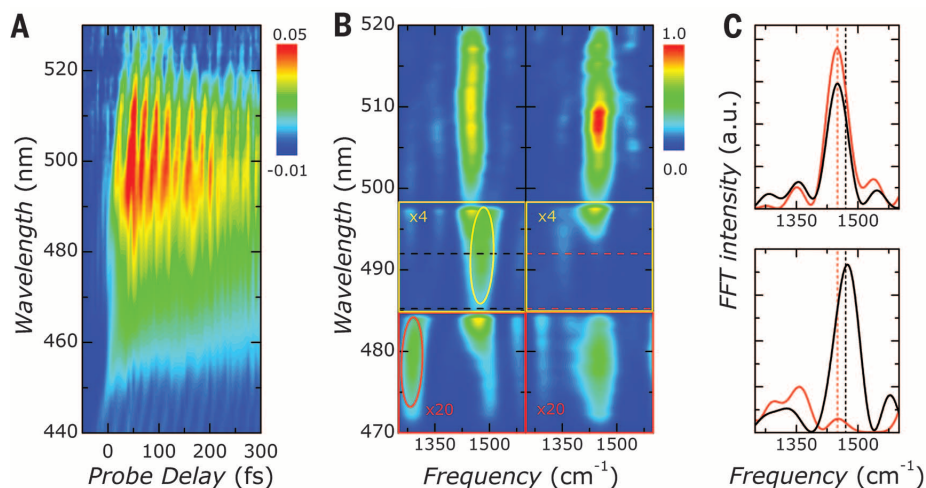


Fig. 2. Charge transfer dynamics of the P3HT:PCBM blend. (A) Experimental differential transmission ($\Delta T/T$) map of the P3HT:PCBM blend as a function of probe delay and probe wavelength. The pronounced oscillations in the $\Delta T/T$ signal reflect coherent vibrational wave-packet motion initiated by the short pump pulse. (B) Fourier transform spectra of the $\Delta T/T$ dynamics of the blend (left) and pristine P3HT (right). The spectral intensity is amplified by a factor of 4 for $\lambda = 498$ to 485 nm and by a factor of 20 for $\lambda = 485$ to 470 nm. (C) Integrated Fourier transform spectra for $\lambda = 520$ to 498 nm (top) and $\lambda = 492$ to 485 nm [bottom, dashed lines in (B)] of the blend (black) and pristine P3HT (red). The dashed vertical lines indicate the frequency of the P3HT C=C stretch mode (red) at 1450 cm^{-1} and pentagonal-pinch mode of the fullerene (black) at 1470 cm^{-1} .

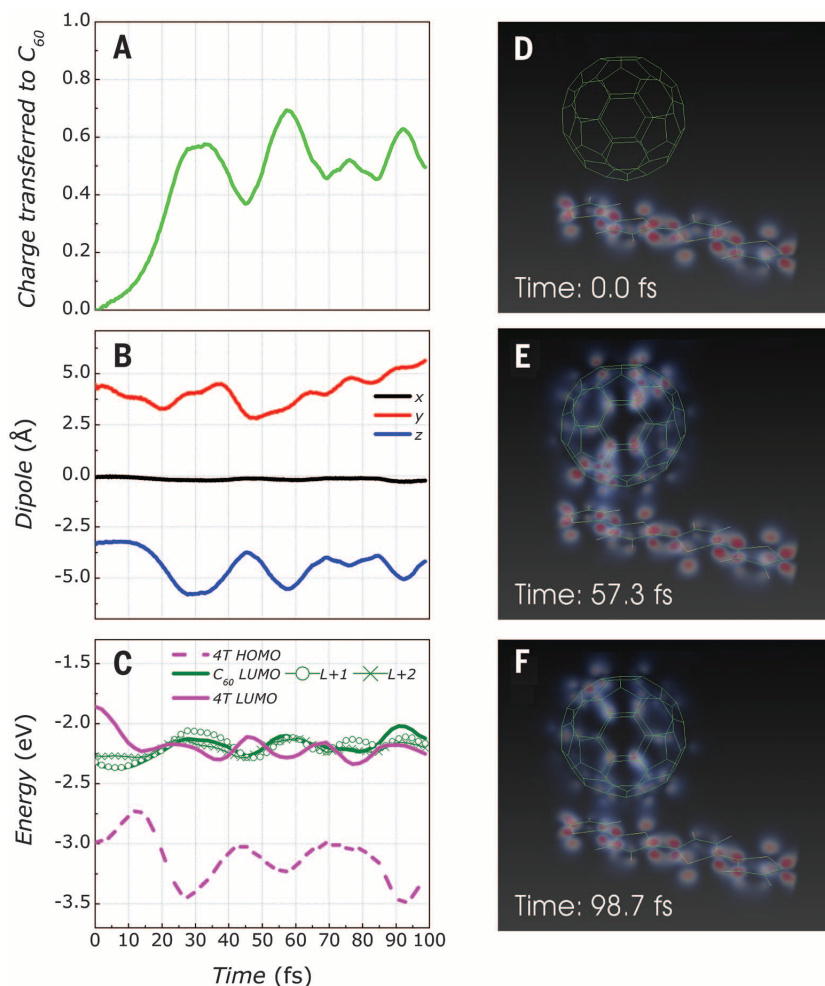


Fig. 3. Simulation of the charge transfer dynamics. (A) Charge-transfer dynamics in a crystal of 4T:C60 aggregates after impulsive 4T excitation at time zero. After 97 fs, the charge-transfer probability from 4T to C₆₀ is 60%. Strong oscillations of the transfer probability, with a period of about 25 ± 4 fs, are the signature of coherent charge-transfer dynamics. (B) Time dynamics of the molecular dipole. The z component, oriented along the axis from the 4T to the C₆₀, oscillates in phase with the displaced charge. (C) Time-dependent Kohn-Sham eigenvalues. The purple lines refer to the 4T HOMO (broken) and 4T LUMO (solid) levels; the green lines to the lowest unoccupied C₆₀ levels, respectively. (D to F) Snapshots of the simulated time evolution of the charge density in the coupled 4T and C₆₀ LUMOs. Initially (D), the charge is completely localized on the 4T chain. As time evolves, it delocalizes between 4T and C₆₀ [(E) 57.3 fs]. After 98.7 fs (F), the charge density is shared between 4T and C₆₀.

We recently studied the charge-transfer dynamics in a very different system, a supramolecular carotene-porphyrin-fullerene triad (24), a model system for artificial light harvesting. The physical nature of this system, a covalently bound molecular complex in solution, is fundamentally different from the one studied here. Nevertheless, we find similar charge oscillations, with a period of about 30 fs, when studying the charge transfer between porphyrin and fullerene. We believe that the key to the similarity of those values can be found in Fig. 3C. It shows that the energies of the relevant LUMOs of the polymer and fullerene vary in time with a period corresponding to that of the vibrational mode to which the electronic state is strongly coupled. The probability for charge transfer is large whenever the polymer and fullerene LUMOs

are transiently brought into resonance. Hence, the amount of transferred charge (Fig. 3A) oscillates at the (average) period of the vibrational mode(s) most strongly coupled to the electronic system.

In case of the P3HT:PCBM blend, these are the C=C stretch mode of the polymer at 1450 cm^{-1} and the pentagonal pinch mode of PCBM at 1470 cm^{-1} , corresponding to an oscillation period of ~ 23 fs. This agrees reasonably well with the period of 25 ± 4 fs that we deduce from Fig. 3, A to C. This period is slightly shorter than the 30 fs that we saw in the case of the triad.

We suggest that the similarity of oscillation periods is a direct consequence of strong vibronic coupling. The time evolution of the charge distribution is modulated with a period matching that of the vibrational modes that are most strongly

coupled to the charge excitations. Because all carbon-based organic systems have strong vibrations in the 1000 to 1500 cm^{-1} range, it is likely to experimentally find oscillation periods between 20 and 30 fs. Our results suggest that, despite the very different microscopic properties of the triad and the P3HT:PCBM blend, the coherent charge-transfer dynamics are in both cases governed by strong vibronic coupling.

A consistent and general picture of the elementary photoinduced charge-transfer process in the P3HT:PCBM blend emerges from our detailed experimental and theoretical results. Optical excitation locally creates an electron-hole pair on the polymer moiety. The strong vibronic coupling between electronic and nuclear degrees of freedom promotes a delocalization of the optically excited electronic wave packet across the interface. Both the electronic density and the nuclei display correlated oscillations on the same time scales, which are essential for an ultrafast charge transfer from the donor to the acceptor. The observation of coherent electron-nuclear motion in a noncovalently bound complex, averaging over a macroscopic ensemble of P3HT:PCBM moieties with variable environment and interfaces, is strong evidence for the dominant role of quantum coherences in the early stages of the charge transfer dynamics in this class of OPV materials.

REFERENCES AND NOTES

1. G. Yu, J. Gao, J. C. Hummelen, F. Wudl, A. J. Heeger, *Science* **270**, 1789–1791 (1995).
2. C. J. Brabec *et al.*, *Adv. Mater.* **22**, 3839–3856 (2010).
3. I.-W. Hwang, D. Moses, A. J. Heeger, *J. Phys. Chem. C* **112**, 4350–4354 (2008).
4. M. Hallermann, S. Haneder, E. Da Como, *Appl. Phys. Lett.* **93**, 053307–053303 (2008).
5. C. J. Brabec *et al.*, *Chem. Phys. Lett.* **340**, 232–236 (2001).
6. N. S. Saricicfti, L. Smilowitz, A. J. Heeger, F. Wudl, *Science* **258**, 1474–1476 (1992).
7. J. Guo, H. Ohkita, H. Benten, S. Ito, *J. Am. Chem. Soc.* **132**, 6154–6164 (2010).
8. I. A. Howard, R. Mauer, M. Meister, F. Laquai, *J. Am. Chem. Soc.* **132**, 14866–14876 (2010).
9. I. W. Hwang *et al.*, *Adv. Mater.* **19**, 2307–2312 (2007).
10. G. Grancini *et al.*, *Nat. Mater.* **12**, 29–33 (2013).
11. R. A. Marcus, *Angew. Chem. Int. Ed. Engl.* **32**, 1111–1121 (1993).
12. A. A. Bakulin *et al.*, *Science* **335**, 1340–1344 (2012).
13. A. E. Jaiilabekov *et al.*, *Nat. Mater.* **12**, 66–73 (2013).
14. L. Pandey, C. Risko, J. E. Norton, J.-L. Brédas, *Macromolecules* **45**, 6405–6414 (2012).
15. Y. Kanai, Z. Wu, J. C. Grossman, *J. Mater. Chem.* **20**, 1053–1061 (2010).
16. J. Ren, S. Meng, E. Kaxiras, *Nano Res.* **5**, 248–257 (2012).
17. H. Tamura, R. Martinazzo, M. Ruckebauer, I. Burghardt, *J. Chem. Phys.* **137**, A540 (2012).
18. H. Tamura, I. Burghardt, M. Tsukada, *J. Phys. Chem. C* **115**, 10205–10210 (2011).
19. H. Tamura, I. Burghardt, *J. Phys. Chem. C* **117**, 15020–15025 (2013).
20. H. Lee, Y. C. Cheng, G. R. Fleming, *Science* **316**, 1462–1465 (2007).
21. E. Collini *et al.*, *Nature* **463**, 644–647 (2010).
22. G. D. Scholes, G. R. Fleming, A. Olaya-Castro, R. van Grondelle, *Nat. Chem.* **3**, 763–774 (2011).
23. E. Collini, G. D. Scholes, *Science* **323**, 369–373 (2009).
24. C. A. Rozzi *et al.*, *Nat. Commun.* **4**, 1602 (2013).
25. S. Gélinas *et al.*, *Science* **343**, 512–516 (2014).
26. G. Dennler, M. C. Scharber, C. J. Brabec, *Adv. Mater.* **21**, 1323–1338 (2009).
27. M. T. Dang, L. Hirsch, G. Wantz, *Adv. Mater.* **23**, 3597–3602 (2011).

28. W. Ma, C. Yang, X. Gong, K. Lee, A. J. Heeger, *Adv. Funct. Mater.* **15**, 1617–1622 (2005).
29. S. Cook, R. Katoh, A. Furube, *J. Phys. Chem. C* **113**, 2547–2552 (2009).
30. J. Clark, C. Silva, R. H. Friend, F. C. Spano, *Phys. Rev. Lett.* **98**, 206406 (2007).
31. W. J. D. Beenken *et al.*, *Phys. Chem. Chem. Phys.* **15**, 16494–16502 (2013).
32. C. Manzoni, D. Polli, G. Cerullo, *Rev. Sci. Instrum.* **77**, 023103 (2006).
33. W. J. Grzegorzczak *et al.*, *J. Phys. Chem. C* **114**, 5182–5186 (2010).
34. P. J. Brown *et al.*, *Phys. Rev. B* **67**, 064203 (2003).
35. D. S. Bethune, G. Meijer, W. C. Tang, H. J. Rosen, *Chem. Phys. Lett.* **174**, 219–222 (1990).
36. S. Falke, P. Eravuchira, A. Materny, C. Lienau, *J. Raman Spectrosc.* **42**, 1897–1900 (2011).
37. X. Andrade *et al.*, *J. Chem. Theory Comput.* **5**, 728–742 (2009).
38. A. Castro *et al.*, *Phys. Status Solidi B Basic Res.* **243**, 2465–2488 (2006).

ACKNOWLEDGMENTS

Financial support by the European Union project CRONOS (grant number 280879-2), the Deutsche Forschungsgemeinschaft (SPP1391), the Korea Foundation for International Cooperation of Science and Technology (Global Research Laboratory project, K2081500003), and the Italian Fondo per gli Investimenti della Ricerca di Base (Flashit project) is gratefully acknowledged. C.A.R. and E.M. acknowledge the Partnership for Advanced Computing in Europe (project LAIT) for awarding us access to supercomputing resources at CINECA, Italy, and useful discussions with C. Cocchi and Y. Kanai. S.M.F. is grateful for a Ph.D. fellowship from Stiftung der Metallindustrie im Nord-Westen. C.L. and G.C. acknowledge support from the European Community (Seventh Framework Programme INFRASTRUCTURES-2008-1, Laserlab Europe II contract no. 228334); A.R. acknowledges financial support from the European Research Council (ERC-2010-AdG-267374), Spanish grant (FIS2010-21282-C02-01), Grupos Consolidados (IT578-13), Ikerbasque. G.C. acknowledges financial support by the European Research Council (ERC-2011-AdG no. 291198). C.L., S.M.F., G.C., C.A.R., and E.M. initiated this

work. S.M.F. prepared the samples. S.M.F., D.B., M.M., E.S., and A.D.S. performed the ultrafast spectroscopy experiments. C.A.R. and M.A. performed DFT and TDDFT simulations. S.M.F., A.D.S., D.B., G.C., and C.L. analyzed and discussed the experimental data. C.A.R., M.A., E.M., and A.R. analyzed and discussed the theoretical data. C.A.R., E.M., G.C., A.D.S., and C.L. designed the paper. All authors discussed the implications and contributed to the writing of the paper. The authors declare no competing financial interests.

SUPPLEMENTARY MATERIALS

www.sciencemag.org/content/344/6187/1001/suppl/DC1
Materials and Methods
Supplementary Text
Figs. S1 to S10
References (39–48)
Movies S1 and S2

16 December 2013; accepted 7 May 2014
10.1126/science.1249771

WATER SPLITTING

Amorphous TiO₂ coatings stabilize Si, GaAs, and GaP photoanodes for efficient water oxidation

Shu Hu,^{1,2} Matthew R. Shaner,^{1,2} Joseph A. Beardslee,¹ Michael Lichterman,^{1,2} Bruce S. Brunschwig,³ Nathan S. Lewis^{1,2,3,4*}

Although semiconductors such as silicon (Si), gallium arsenide (GaAs), and gallium phosphide (GaP) have band gaps that make them efficient photoanodes for solar fuel production, these materials are unstable in aqueous media. We show that TiO₂ coatings (4 to 143 nanometers thick) grown by atomic layer deposition prevent corrosion, have electronic defects that promote hole conduction, and are sufficiently transparent to reach the light-limited performance of protected semiconductors. In conjunction with a thin layer or islands of Ni oxide electrocatalysts, Si photoanodes exhibited continuous oxidation of 1.0 molar aqueous KOH to O₂ for more than 100 hours at photocurrent densities of >30 milliamperes per square centimeter and ~100% Faradaic efficiency. TiO₂-coated GaAs and GaP photoelectrodes exhibited photovoltages of 0.81 and 0.59 V and light-limiting photocurrent densities of 14.3 and 3.4 milliamperes per square centimeter, respectively, for water oxidation.

The oxidation of water to O₂ is a key process in the direct photoelectrochemical (PEC) production of fuels from sunlight (1, 2). A fuel-forming reductive half-reaction involving the reduction of CO₂ to lower hydrocarbons or the reduction of H₂O to H₂ requires an oxidative half-reaction, such as the oxidation of water to O₂. Metal oxide photoanodes can oxidize water to O₂ in alkaline or acidic media, but thus far have been inefficient because their band gaps are too large and because the potential of their valence band edge is much more positive than the formal potential

for water oxidation, E^o(O₂/H₂O) (3). Although many semiconductors, including silicon (Si), gallium arsenide (GaAs), and gallium phosphide (GaP), have valence-band edges at more negative potentials than metal oxides and also typically have optimal band gaps for efficient solar-driven water splitting, these semiconductors are unstable when operated under photoanodic conditions in aqueous electrolytes. Specifically, in competition with oxidizing water to O₂, these materials either anodically photocorrode or photopassivate (3, 4). Furthermore, passive and intrinsically safe solar-driven water-splitting systems can only be constructed (5) in either alkaline or acidic media, and the development of general strategies to stabilize existing photoelectrode materials under water-oxidation conditions is an important goal.

Various coating strategies have been explored to stabilize semiconductors with optimal band gaps (1.1 to 1.7 eV) for direct water splitting (6).

Deposition of thin films of Pd (7), Pt (8), Ni (9), or metal-doped SiO_x (10) onto n-type Si or n-GaAs photoanodes yields improved stability under water-oxidation conditions, primarily near neutral pH, as well as in strongly alkaline (9) or acidic (10) media for up to 12 hours. However, these stabilized photoanodes generally exhibit low photovoltages; additionally, the protective metal coating is either too thick to be highly optically transmissive or too thin to afford extended stability during water oxidation, particularly in alkaline or acidic media. Transparent conductive oxide (TCO) coatings on Si and GaAs are not stable in strongly alkaline or acidic media, and also produce low voltages because of defective semiconductor/TCO interfaces. (11, 12) Coatings of Ni islands (9), as well as MnO_x (13) and NiO_x (14) films on Si, have been used to catalyze the oxidation of water and thus provide some degree of stability enhancement. However, such coatings do not enable prolonged operation in alkaline media and/or yield very low photovoltages because of a large density of interface states at the Si/Ni interface.

Conformal layers of 2-nm thin TiO₂ formed by atomic layer deposition (ALD) have been used to stabilize Si, and in conjunction with an IrO_x catalyst, to effect water oxidation (15). Deposition of such electrically insulating films at larger thickness, to reliably prevent pinholes and thus suppress active corrosion over macroscopic areas, creates a tunneling barrier for photogenerated holes. As this barrier becomes thicker, it no longer conducts holes via a tunneling mechanism and also introduces a large series resistance to a PEC device, degrading its efficiency to low values. Specifically, as the TiO₂ thickness was increased, the overpotential for the oxygen-evolution reaction (OER) increased linearly at a rate of ~21 mV nm⁻¹ (16), resulting in an additional voltage loss of ~200 mV for a 12-nm thick TiO₂ overlayer, even at a current density of 1 mA cm⁻².

We describe a general approach to significantly improve the stability of Si, GaAs, and GaP photoanodes against both photocorrosion and photopassivation for water oxidation in alkaline media [all results reported below are

¹Division of Chemistry and Chemical Engineering, California Institute of Technology, Pasadena, CA 91125, USA. ²Joint Center for Artificial Photosynthesis, California Institute of Technology, Pasadena, CA 91125, USA. ³Beckman Institute and Molecular Materials Research Center, California Institute of Technology, Pasadena, CA 91125, USA. ⁴Kavli Nanoscience Institute, California Institute of Technology, Pasadena, CA 91125, USA.

*Corresponding author. E-mail: nslewis@caltech.edu